Published in final edited form as:
Neurobiol Aging. 2014 July ; 35(7): 1549–1561. doi:10.1016/j.neurobiolaging.2014.01.144.

Ex vivo T_2 relaxation: Associations with age-related neuropathology and cognition

Robert J. Dawe[a,b], **David A. Bennett**[a,c], **Julie A. Schneider**[a,c,d], **Sue E. Leurgans**[a,c], **Aikaterini Kotrotsou**[e], **Patricia A. Boyle**[a,f], and **Konstantinos Arfanakis**[a,b,e]

[a]Rush Alzheimer's Disease Center, Rush University Medical Center, Chicago, Illinois, USA

[b]Department of Diagnostic Radiology and Nuclear Medicine, Rush University Medical Center, Chicago, Illinois, USA

[c]Department of Neurological Sciences, Rush University Medical Center, Chicago, Illinois, USA

[d]Department of Pathology, Rush University Medical Center, Chicago, Illinois, USA

[e]Department of Biomedical Engineering, Illinois Institute of Technology, Chicago, Illinois, USA

[f]Department of Behavioral Sciences, Rush University Medical Center, Chicago, Illinois, USA

Abstract

The transverse relaxation time constant, T_2, is sensitive to brain tissue's free water content and the presence of paramagnetic materials such as iron. In this study, ex vivo MRI was employed to investigate alterations in T_2 related to Alzheimer's disease (AD) pathology and other types of neuropathology common in old age, as well as the relationship between T_2 alterations and cognition. Cerebral hemispheres were obtained from 371 deceased older adults. Using fast spin-echo imaging with multiple echo times, T_2 maps were produced and warped to a study-specific template. Hemispheres underwent neuropathologic examination for identification of AD pathology and other common age-related neuropathologies. Voxelwise linear regression was carried out to detect regions of pathology-related T_2 alterations and, in separate analyses, regions in which T_2 alterations were linked to antemortem cognitive performance. AD pathology was associated with T_2 prolongation in white matter of all lobes and T_2 shortening in the basal ganglia and insula. Gross infarcts were associated with T_2 prolongation in white matter of all lobes, and in the thalamus and basal ganglia. Hippocampal sclerosis was associated with T_2 prolongation in the hippocampus and white matter of the temporal lobe. After controlling for neuropathology, T_2 prolongation in the frontal lobe white matter was associated with lower performance in the episodic, semantic, and working memory domains. In addition, voxelwise analysis of in vivo and ex vivo T_2 values indicated a positive relationship between the two, though further investigation is necessary to accurately translate findings of the current study to the in vivo case.

Corresponding author: Konstantinos Arfanakis, PhD, 3440 S. Dearborn St., Medical Imaging Research Center, M-102, Chicago, IL 60616, phone: (312) 567-3864, fax: (312) 567-3225, arfanakis@iit.edu.

Keywords

Neuroimaging; MRI; gross infarct; hippocampal sclerosis; cognition; voxelwise

1 Introduction

The transverse relaxation time constant, T_2, describes the decay rate of the transverse component of magnetization due to irreversible dephasing, and is one of the main sources of contrast available in MRI. For H1 imaging at a given field strength, T_2 is influenced by a number of factors, including the ratio of free to myelin-bound water molecules (House et al., 2006), and the presence of paramagnetic molecules, such as the iron-laden compounds ferritin and hemosiderin (Haacke et al., 2005). Various types of pathology can alter these tissue properties and consequently change T_2 values. For this reason, T_2 has the potential to serve as a biomarker for a range of diseases, and studies that investigate the relationships between pathology, cognition, and T_2 are warranted.

Alzheimer's disease (AD) is one such condition for which T_2 alterations have been observed in different regions of the brain. Several studies have reported a significant increase in hippocampal T_2 in individuals with AD compared to controls (Arfanakis et al., 2007, Kirsch et al., 1992, Laakso et al., 1996, Wang et al., 2004), and this is thought to be attributable to neuronal loss (West et al., 1994) and a resulting increase in the tissue's water content. However, other studies that examined the hippocampus did not find significant alterations in T_2 in individuals with mild to severe cognitive impairment (House et al., 2006) or in histopathologically confirmed cases of AD (House et al., 2008). Outside of the hippocampus, elevated T_2 times have been reported in the internal capsule and in the frontal, temporal, and parahippocampal white matter of individuals with clinically or pathologically diagnosed AD and those with memory complaints or mild to severe cognitive impairment, a phenomenon which some attribute to the breakdown of myelin and the resultant increase in the tissue's free water content (Bartzokis et al., 2003, Besson et al., 1992, House et al., 2006). T_2 prolongation has also been reported in the amygdala of individuals with AD (Wang et al., 2004). Significantly reduced T_2 times thought to result from iron accumulation have been detected in the temporal lobe gray matter of living individuals reporting memory loss (House et al., 2006). By contrast, a related study of postmortem brain tissue did not find a significant T_2 reduction in temporal lobe gray matter in histopathologically confirmed cases of AD (House et al., 2008).

While these findings shed light on a potentially important relation of T_2 to AD, the majority of the studies did not have the benefit of a neuropathologic index or diagnosis of AD, and instead relied only on clinical diagnosis. Even in those few studies that combined measurements of T_2 with pathologic diagnosis of AD, common coexisting age-related pathologies, such as infarcts, were rarely included in the analyses. Further, we are not aware of prior studies which have examined the clinical significance of T_2 alterations by investigating their relation to cognitive status proximate to death, while also controlling for the effects of pathology. Therefore, several gaps in our knowledge of T_2 alterations related to AD and other common neuropathologies in the human brain remain to be filled.

To address these issues, it is necessary to combine clinical data with neuropathology and imaging data from the same human brain tissue via one of two methods. One approach involves conducting MRI during life, and then, upon death of those individuals, examining the brain tissue histopathologically. The other approach, the one adopted in the current study, avoids a potentially lengthy delay between MRI and death by subjecting ex vivo human brain specimens to MRI, followed by histopathologic examination. This second approach eliminates the possible confound of additional neuropathology formation between MRI and histopathologic examination, since both procedures are performed postmortem. It also permits assessment of the large number of cerebral hemispheres necessary to examine the range of pathologies across the spectrum of cognitive function.

The purpose of this study was to conduct a cerebrum-wide analysis of T_2 alterations associated with AD pathology, Lewy bodies, microscopic infarcts, gross infarcts, and hippocampal sclerosis (HS). We also investigated whether T_2 alteration is associated with cognitive function beyond that accounted for by neuropathology. The investigations were carried out by employing ex vivo MRI to map T_2 values in human cerebral hemispheres from nearly 375 individuals, followed by histopathological examination of the same specimens. All brain hemispheres were obtained from study participants whose cognition had been assessed proximate to death. By accounting for the aforementioned types of neuropathology in a combined multiple linear regression, it was possible to study the T_2 alterations associated with each condition, something that has not been accomplished previously in either ROI-based or voxel-based analyses. Additional voxelwise regression was carried out to assess the contribution of T_2 to variation in cognitive measures, while also considering the association of cognition with neuropathologic indices.

2 Materials and Methods

2.1 Ethics Statement

Older adults included in this work were participants in one of two longitudinal clinical-pathologic studies of aging: the Rush Memory and Aging Project (MAP) or the Religious Orders Study (ROS) (Bennett et al., 2012a, Bennett et al., 2012b). All participants provided written informed consent and signed an anatomical gift act. The study was approved by the Institutional Review Board of Rush University Medical Center.

2.2 Brain Hemispheres

In a period of six years, 395 individuals from the MAP and ROS projects who died were considered for inclusion in this study. After a participant's death, autopsy technicians removed and separated the cerebral hemispheres as previously described (Dawe et al., 2011). One hemisphere per participant was selected for ex vivo imaging, and this hemisphere was immersed in phosphate-buffered 4% formaldehyde solution (prepared from paraformaldehyde) and refrigerated at 4° C in a sealed plastic container within an hour of its removal from the skull.

2.3 Ex Vivo Image Acquisition and Processing

MRI scans occurred at 47 ± 25 days (mean ± standard deviation) postmortem (range 22–235) (Dawe et al., 2009). All scans were performed with the hemisphere immersed in room temperature formaldehyde solution in a clear, sealed acrylic container. Due to the ongoing nature of this imaging study, three different scanners were used to acquire fast spin-echo MRI data with at least two different echo times (TEs): a General Electric Signa scanner (Waukesha, WI, USA) was used from 2006 to 2008, a Siemens Trio (Erlangen, Germany) from 2008 to 2010, and a Philips Achieva (Best, The Netherlands) after 2010. While all three scanners had the same nominal field strength (3 Tesla) and approximately the same scan time (31–35 minutes), other factors varied among the scanners, including details of the fast spin-echo sequence (Table 1). The last two echoes from the Philips scanner (66 ms and 82.5 ms) were discarded in order to maintain a similar range of echo times across all three scanners.

For a given postmortem hemisphere, a T_2 image volume was estimated from the set of images generated from the multiple echo times (Fig. 1). This was accomplished by fitting the equation $S_i = S_0 \exp(-TE_i/T_2)$ to the data using a least squares approach, where S_i is the signal measured at TE_i, and S_0 is the fitted signal extrapolated to a proton density weighting at TE = 0 ms. The resulting S_0 and T_2 maps were masked at a T_2 value of 150 ms to eliminate the long-T_2 formaldehyde solution from the T_2 image volumes. For hemispheres from the left side of the brain, the slice order was reversed so that they appeared as right hemispheres in all subsequent analyses. Of the 395 hemispheres undergoing MRI, 24 were found to have gross abnormalities, such as tumors or large hemorrhages, precluding accurate spatial normalization. These hemispheres were removed from the analysis, leaving 371 total hemispheres.

2.4 Study-Specific Template Creation

Of the remaining 371 hemispheres, 30 were used to generate a study-specific template. These 30 hemispheres were chosen to span the range of AD pathology burden (see Section 2.6, Neuropathologic Evaluation), from minimal to severe, so as to avoid bias toward a particular level of AD pathology. Half came from male participants, and the mean ages at death were matched between males and females. The high dimensional warping algorithm of the Automatic Registration Toolbox (ART) (Ardekani et al., 2005) was used to spatially normalize the 30 hemispheric S_0 image volumes in an iterative fashion (Joshi et al., 2004). The final template was produced by calculating the mean of the 30 S_0 volumes and is visible in Figures 2 through 6, in which it serves as the grayscale underlay.

2.5 Spatial Normalization of Individual Hemispheres

Using ART, the S_0 volume from each brain hemisphere was warped to match the template. The deformation field map defining this transformation was then applied to that same hemisphere's T_2 volume. Thus, all 371 T_2 volumes became spatially normalized to an unbiased template via a high dimensional transformation, facilitating voxelwise analyses.

2.6 Neuropathologic Evaluation

Following MRI, each cerebral hemisphere was placed in a Plexiglas jig and cut coronally into 1-cm thick slabs. Slabs underwent complete macroscopic evaluation and dissection of blocks, including midfrontal, middle temporal, inferior parietal, and entorhinal cortices, hippocampus, anterior basal ganglia, anterior thalamus, and midbrain, including substantia nigra. These regions were embedded in paraffin, cut into sections, and mounted on glass slides. Brain autopsy procedures have been described previously (Schneider et al., 2009).

Neuropathologic assessments were completed by a board-certified neuropathologist blinded to age and all clinical data. Bielschowsky silver stain was used to visualize neuritic plaques, diffuse plaques, and neurofibrillary tangles in the frontal, temporal, parietal, and entorhinal cortices and the hippocampus. Plaque and tangle counts were converted to standardized scores in each area. Summary scores for each marker were then computed by averaging across the five regions. Finally, these three summary scores were averaged to produce a global measure of AD pathology for each hemisphere. Details of the evaluation of AD pathology and computation of the global score have been described previously (Schneider et al., 2007). For descriptive purposes only, a neuropathologic diagnosis of low, intermediate, or high AD pathology was also rendered, based on the Braak score for neurofibrillary pathology and the CERAD estimate of neuritic plaques, as recommended by the NIA-Reagan criteria (The National Institute on Aging, and Reagan Institute Working Group on Diagnostic Criteria for the Neuropathological Assessment of Alzheimer's Disease, 1997), but modified to exclude clinical diagnosis. Lewy bodies were identified with antibodies to alpha-synuclein (Schneider et al., 2009) and were classified as limbic or neocortical based on recommended guidelines (McKeith, 2006). The brain and slabs were examined for gross cerebral infarcts (infarcts visualized by the naked eye) as previously described (Schneider et al., 2009). For analyses, the total number of gross infarcts was recorded, as well as each infarct’s age (acute, subacute, or chronic). Microscopic infarcts (defined as infarcts seen microscopically but not macroscopically) were counted on 6-micron hematoxylin and eosin-stained routine sections (Arvanitakis et al., 2011) and were also classified by age. Hippocampal sclerosis was defined as substantial neuronal loss and gliosis including the hippocampal CA1 sector, as assessed on 6-micron sections (Dawe et al., 2011).

2.7 Assessment of Cognitive Performance

The two longitudinal studies from which participants originated (MAP and ROS) have 19 cognitive tests in common. Of those, the Mini-Mental State Examination (MMSE) is used for descriptive purposes, and one other test, Complex Ideational Material, is only used in diagnostic classification. The remaining 17 tests assess a broad range of cognitive abilities. The scores from those 17 tests are converted to z-scores based on the mean and standard deviation at baseline, and combined to obtain measures of five cognitive domains: episodic memory, semantic memory, working memory, perceptual speed, and visuospatial ability. Details of the cognitive tests and the use of combined measures from both cohorts have been previously described (Bennett et al., 2006, Bennett et al., 2009, Wilson et al., 2007).

2.8 Voxelwise Statistical Analysis

Custom software written in Matlab (The Mathworks, Inc., Natick, MA) was used to conduct voxelwise linear regression. First, each type of pathology was considered separately to assess its potential association with T_2 in each voxel (i.e., one voxelwise regression for each type of pathology, with T_2 as the outcome variable). Subsequently, a combined voxelwise regression was conducted in which those types of pathology found to have significant associations with T_2 were simultaneously entered in the model. Each regression model included terms to account for the postmortem interval to MRI (Dawe et al., 2009), the scanner used to acquire images from each hemisphere (GE, Siemens, or Philips), participant's age at death (Hasan et al., 2010), sex (Kumar et al., 2012), and years of education.

A separate analysis was then performed to investigate the possible association of T_2 with cognition. For each of five cognitive domains, a series of regression analyses were carried out with cognitive score as the outcome variable. First, only demographics were included as explanatory variables. The five types of neuropathology were then included, with acute and subacute infarcts (both gross and microscopic) held out of the analysis since most participants likely underwent cognitive assessment prior to sustaining these. Finally, voxelwise T_2 was added as an explanatory variable. The explained percentage of variance in cognition was computed for each addition of explanatory variables to the model.

For all voxelwise regression analyses conducted throughout the study, voxels for which the explanatory factor of interest had significant association with the outcome variable (either T_2 or cognitive score) were identified by masking the raw p-value maps at a threshold expected to produce a false discovery rate (FDR) of 5% ('fdr' tool of the FSL software package, http://www.fmrib.ox.ac.uk/fsl/). To further guard against Type I errors, only voxels belonging to clusters greater than 100 mm^3 in volume were ultimately considered to be statistically significant. The FDR-adjusted and clustered p-value maps were used to mask colorized contrast maps, which were then overlaid on the template volume in AFNI for visualization (Cox, 1996).

2.9 Addressing Inter-Scanner Variation in T_2

We guarded against spurious findings stemming from systematic variation in T_2 among scanners in two ways. First, as mentioned in the preceding section, we included binary explanatory variables in each regression model to code for the scanner used to image each hemisphere, allowing constant, voxelwise offsets in T_2 among the three different instruments. Second, we repeated all voxelwise analyses on the largest subgroup of hemispheres imaged on a single scanner (Philips Achieva, 188 hemispheres) and compared these results to the findings of the full analysis. An incidental benefit of the single scanner analysis was a marked reduction in the variance and range of postmortem intervals to MRI compared to the full analysis (mean ± standard deviation of 35 ± 7.1 days, range of 24–58 days), meaning that a potential contribution from this factor was effectively minimized.

2.10 Generalization of Ex Vivo Findings

To explore the potential for extrapolation of ex vivo imaging findings to the in vivo case, we investigated the relationship between in vivo and ex vivo T_2 values. T_2 maps were calculated for 28 living participants in the MAP and ROS studies who had undergone multi-spin echo MRI in a 3-Tesla scanner (Siemens Trio, Erlangen, Germany) using the following parameters: TE = 20/40/60/80/100 ms, TR = 5.7 s, field of view = 183 × 230 mm, acquisition matrix = 143 × 256, slice thickness = 3 mm, parallel imaging factor = 2, and a single average. These in vivo T_2 maps were spatially warped to a common template along with ex vivo T_2 maps from 28 age- and sex-matched brain donors. Spherical ROIs were selected in white matter (at least one ROI in each lobe) and in two well-registered subcortical gray matter regions, the putamen and globus pallidus. ROIs were not selected in cortical gray matter due to reduced registration accuracy of cortical areas across subjects. For each voxel, the mean ex vivo T_2 was plotted against the corresponding mean in vivo T_2. Linear regression was carried out per ROI to assess the relationship between ex vivo and in vivo T_2.

3 Results

3.1 Participant Demographics and Neuropathology

Characteristics of the 371 participants/hemispheres are summarized in Table 2. AD (either intermediate or high NIA-Reagan score) was the most commonly observed neuropathology, followed by chronic microscopic and chronic gross infarcts. Hippocampal sclerosis and Lewy bodies were less common, but were still observed in more than 20% of the hemispheres. Subacute and acute infarcts (both microscopic and gross) were relatively rare, each observed in 11% or fewer of the hemispheres.

3.2 Association of T_2 with Neuropathology

In the voxelwise regression analyses in which only one type of neuropathology was considered at a time, statistically significant associations with T_2 were detected for the global summary score of AD pathology, chronic and acute gross infarcts, and hippocampal sclerosis. Therefore, these four types of pathology were entered in a combined regression model for further analysis. No regions with significant T_2 alterations were observed in association with subacute gross infarcts, microscopic infarcts of any age, or Lewy bodies, after FDR adjustment of voxelwise p-values.

3.2.1 Alzheimer's Disease—In the combined regression (multiple types of neuropathology considered simultaneously), the global AD pathology measure was associated with significant T_2 alterations in eight separate clusters throughout the hemisphere (Table 3, Fig. 2). The largest two clusters exhibited T_2 prolongation and included large portions of the white matter in all four lobes. The remaining six smaller clusters exhibited T_2 shortening in the insula, caudate, globus pallidus, the medial portion of the thalamus, and around the edges of the hippocampus and temporal lobe.

3.2.2 Chronic Gross Infarcts—Chronic gross infarcts were associated with a large cluster of significant T_2 prolongation (Table 3, Fig. 3). This single continuous cluster

engulfed nearly all of the frontal and parietal lobe white matter, sizable portions of the white matter in the occipital and temporal lobes, the putamen, the lateral globus pallidus, and parts of other regions, including the corpus callosum, thalamus, caudate, and medial globus pallidus.

3.2.3 Acute Gross Infarcts—Acute gross infarcts were associated with T_2 prolongation in five separate clusters (Table 3, Fig. 4). The largest cluster included sizable portions of the frontal and parietal lobe white matter, with confluence into the superior temporal white matter, putamen, caudate, and posterior portion of the thalamus. The remaining four clusters included a smaller portion of the frontal and parietal lobe white matter, tissue in or near the cingulum, and white and gray matter near the parietal-occipital border.

3.2.4 Hippocampal Sclerosis—Three clusters of significant T_2 alteration were observed in association with hippocampal sclerosis (Table 3, Fig. 5). The two larger clusters exhibited T_2 prolongation and included portions of the hippocampus, amygdala, parahippocampal white matter, and other white matter of the temporal lobe. The third cluster exhibited T_2 shortening and was located at the inferior edge of the temporal lobe.

3.3 Clinical Significance of T_2 Alterations

For voxelwise regression analyses in which cognition was modeled as a function of T_2 and neuropathologic indices, reduced performances in the episodic, semantic, and working memory domains were associated with prolonged values of T_2, primarily in white matter. A single cluster of prolonged T_2 in the temporal lobe white matter and amygdala (Fig. 6) accounted for 5.5% of the variance in episodic memory scores, beyond that explainable by demographics and the neuropathologic indices (Table 4, bottom three rows). Similarly, four significant clusters of prolonged T_2 combined to account for 8.8% of the variance in semantic memory (Table 4). One of these clusters was located in the frontal lobe white matter, while the other three were located in the temporal lobe white matter (Fig. 6). T_2 prolongation in a large frontal lobe white matter cluster and a smaller parietal lobe cluster accounted for 7.7% of the variance in the working memory scores (Table 4, Fig. 6). Significant associations of cognition with T_2 were not observed in the domains of perceptual speed or visuospatial ability after FDR adjustment of p-values. These results were essentially unchanged after exclusion of those participants who had not undergone cognitive testing within one year of death (resulting n = 290, or 78% of the 371 total participants).

3.4 Single Scanner Analysis

The entire set of voxelwise analyses was repeated using only the 188 hemispheres that were imaged on the Philips Achieva scanner (the largest single scanner subgroup, Table 2), and the results were similar to those of the full 371-hemisphere analysis (Supplementary Table 5). Notably, in the 188-hemisphere analysis, a cluster of AD-associated T_2 prolongation was observed within the hippocampus proper, which did not reach the FDR-corrected significance threshold in the full 371-hemisphere analysis. Elsewhere, several clusters of significant T_2 alteration from the full 371-hemisphere analysis appeared only as sub-significant trends in the lower-powered 188-hemisphere analysis.

3.5 Generalization of Ex Vivo Findings

Ex vivo T_2 values were approximately 50% of the corresponding in vivo values. The relationships between ex vivo and in vivo T_2 per ROI are illustrated in Figure 7. Linear relationships with R^2 values greater than 0.71 were detected in all cases ($p < 10^{-15}$). When voxels from all seven regions were pooled in a single analysis, the regression line was described by the equation [ex vivo T_2] = 0.34·[in vivo T_2] + 16.0 ms, and the R^2 value was 0.84 ($p < 10^{-15}$).

4 Discussion

The current study builds on previous research of AD-related T_2 alterations by combining ex vivo brain MRI data with neuropathologic and antemortem cognitive measures. To our knowledge, this study represents the first cerebrum-wide analysis of T_2 effects associated with the histopathology of AD as well as other types of neuropathology commonly found in the brain. In addition, findings regarding associations between cognition and T_2 show that the T_2 prolongations are clinically relevant.

4.1 T_2 Alterations Related to AD

The white matter of the temporal lobe, particularly the temporal stem, exhibited prolonged T_2 in association with AD pathology, as detected by the combined regression that also accounted for other types of neuropathology. In some studies that made similar investigations, AD-related prolongation of T_2 in the temporal lobe white matter was detected in living individuals (House et al., 2006) and in unfixed postmortem tissue (Besson et al., 1992). In the latter case, the prolongation of T_2 was accompanied by a significant increase in the tissue's total water content, leading the authors to surmise that atrophy of the neural component of white matter is responsible for the change in relaxation times. Wallerian-type degeneration has indeed been observed in the temporal white matter of AD brains subjacent to the most severely diseased portion of the cortex (Englund, 1998). In addition, a multitude of diffusion weighted imaging (DWI) and diffusion tensor imaging (DTI) studies have reported increased diffusivity and decreased diffusion anisotropy in temporal lobe white matter of living individuals with clinically diagnosed AD, both of which indicate a reduction of barriers to diffusion (Arfanakis et al., 2007, Bozzali et al., 2002, Hanyu et al., 1998, Huang et al., 2007, Takahashi et al., 2002, Taoka et al., 2006, Wang et al., 2012, Xie et al., 2006).

T_2 prolongation associated with AD was also observed in frontal lobe white matter. This has been reported previously (Bartzokis and Tishler, 2000, Bartzokis et al., 2003, House et al., 2006), though other studies addressing this issue did not detect any significant AD-related T_2 alterations on postmortem MR (Besson et al., 1992, House et al., 2008). The diffuse pattern of this T_2 prolongation, which was most intense toward the deep portions of the frontal white matter and tapered off toward the cortex, convincingly matches the description of white matter disease (WMD) observed in approximately 60% of AD brains (Brun and Englund, 1986, Englund, 1998). Ex vivo MRI has previously been shown to detect this type of white matter abnormality with relatively high sensitivity and specificity (Fernando et al., 2004), presumably owing to the correlation between T_2 and severity of WMD (Englund et

al., 1987). Partial loss of myelin or myelin components with a corresponding increase in the tissue's water content is strongly implicated as the primary biophysical basis of such T_2 prolongation (Englund et al., 1988, Roher et al., 2002, Soderberg et al., 1992). Interestingly, the neuropathologic and biochemical signatures of WMD, including glial changes (Sjobeck and Englund, 2003) and alterations in lipid and protein content (Englund et al., 1988, Roher et al., 2002, Soderberg et al., 1992), bear a striking resemblance to those of the transitional zones surrounding complete infarcts, leading several researchers to theorize that the frontal lobe WMD associated with AD may in fact lie on an axis between normal white matter and fully infarcted white matter (Englund et al., 1988, Sjobeck and Englund, 2003). Furthermore, the pattern of WMD often does not correlate with the spatial distribution of gray matter degeneration in AD (Englund et al., 1988, Roher et al., 2002). Taken together, this information suggests that the frontal lobe T_2 prolongation observed in the current study may stem from a non-Wallerian mechanism of white matter degeneration, with much evidence pointing toward a vascular etiology (Englund et al., 1988, Englund, 1998, Roher et al., 2002, Sjobeck and Englund, 2003). This white matter degeneration, though common in the AD brain, may be decoupled from the disease's hallmark gray matter pathology and degeneration, and as such, may contribute independently to cognitive decline (see Section 4.4).

AD-associated T_2 prolongation was also widespread in the white matter of the parietal and occipital lobes, with apparent confluence into the posterior portion of the cingulum. To the best of our knowledge, such T_2 prolongation in the cingulum has not been reported previously, though a number of DTI studies have shown disruption of diffusion anisotropy and mean diffusivity in the cingulum (especially in the posterior portion) of clinically diagnosed AD patients (Bozzali et al., 2012, Choo et al., 2010, Fellgiebel et al., 2005, Mielke et al., 2009, Takahashi et al., 2002, Zhang et al., 2007). Based on the findings of the current study and supporting DTI evidence from the literature, we surmise that the AD-associated T_2 prolongation in parietal and occipital white matter (including cingulum) is brought about by pathologic processes that ultimately lead to an increase in the tissue's free water content, possibly by the same mechanisms suspected in frontal white matter T_2 prolongation. It is notable that deafferentation of cingulum fibers from the medial temporal lobe has recently been suggested as the progenitor of cingulum disruption in AD (Bozzali et al., 2012).

AD-related alteration of hippocampal T_2 is alluring as a potential biomarker because of the structure's important role in the development of the disease and has been reported in some (though not all) previous studies involving clinically diagnosed living participants (Arfanakis et al., 2007, Kirsch et al., 1992, Laakso et al., 1996, Wang et al., 2004). The results of the current study were inconclusive in this area, as hippocampal T_2 prolongation was detected as a significant alteration in the 188-hemisphere, single scanner regression analysis, but only as a sub-significant trend in the full, 371-hemisphere analysis utilizing three different scanners. In both cases, the effect was positive in sign (i.e. T_2 prolongation), indicating that at 3 T, hippocampal T_2 marker of AD would likely stem from neuronal loss rather than a T_2-shortening effect, such as an abnormal accumulation of iron.

T_2 shortening in association with AD pathology was observed in several relatively small clusters within the cerebral hemisphere. One such cluster included portions of the caudate and globus pallidus. This is a notable finding, given that iron concentrations have been reported to be 78% higher in the globus pallidus of postmortem AD tissue compared to control specimens (Loeffler et al., 1995). Further, ferritin levels in the caudate, putamen, and globus pallidus are elevated in clinically diagnosed AD patients compared to individuals with normal cognition, as indicated by studies employing the field-dependent relaxation rate increase (FDRI) method of iron detection (Bartzokis et al., 1994, Bartzokis et al., 2000).

Significant AD-associated T_2 shortening was also observed in the insula. This appears to be a unique finding not previously described in the literature, although decreased insular T_2*-weighted signal has been reported in patients with mild cognitive impairment and AD (Rombouts et al., 2007). Plaques and tangles, the pathologic hallmarks of AD, and the accompanying iron species (Smith et al., 1997) could potentially be responsible for the observed insular T_2 shortening effect. However, simple calculations show that plaques and tangles alone are unlikely to account for the entire difference in iron concentration in AD brains (House et al., 2008). Instead, it seems that most of the elevation in iron content and consequent T_2 shortening of the tissue may stem from the increased iron concentration of the neuropil in AD (Lovell et al., 1998, Watt, 1996).

Finally, we also detected three ribbon-like clusters of AD-associated T_2 shortening around the edges of the temporal lobe and hippocampus. Based on their location, shape, and large magnitude of T_2 alteration, we speculate that these clusters may be attributable to partial volume effects at the borders of gray matter and non-tissue, rather than a genuine T_2 shortening effect.

4.2 T_2 Alterations Related to Gross Infarcts

Chronic gross infarcts were associated with the most extensive T_2 alterations, by far, of any pathology that was investigated. The large cluster of T_2 prolongation can be described as periventricular in nature, with confluence into deep parenchymal white matter. Although all lobes exhibited at least some T_2 prolongation in white matter, the frontal lobe was the most severely affected region, both in terms of the magnitude of T_2 alteration and the portion of tissue that was affected. The T_2 prolongation associated with gross infarcts is not due to the presence of macroscopic fluid-filled spaces, since these were masked out of individual T_2 maps, effectively removing them from analyses. Instead, the T_2 prolongation detected in association with gross infarcts in the current study may be a manifestation of leukoaraiosis, or white matter rarefaction (observed originally on CT and later extended to MRI) (Inzitari, 2003). The observed pattern of infarct-related T_2 prolongation is qualitatively similar to that seen on T_2-weighted images of severe leukoaraiosis (Fazekas et al., 1993, Inzitari, 2003). While its underlying pathophysiology remains vague, previous research suggests that leukoaraiosis results from selective neuronal loss due to hypoxic but “incomplete” infarction (Auriel et al., 2011, Fernando et al., 2006). In this regard, it is possible that the infarct-related T_2 prolongation shares a similar etiology with the AD-related T_2 prolongation in the frontal lobe (see Section 4.1). Alternatively, the widespread T_2 prolongation in white matter could be due to Wallerian degeneration following infarction, though the pattern appeared to

be global, or diffuse, as opposed to tract-specific. The white matter T_2 prolongation observed in association with acute gross infarcts should be interpreted with caution, since only 12 hemispheres (3% of the total sample) had acute gross infarcts without any accompanying chronic gross infarcts.

4.3 T_2 Alterations Related to Hippocampal Sclerosis

HS is characterized by severe neuronal loss with gliosis in the cornu ammonis 1 (CA1) subregion of the hippocampus (Dickson et al., 1994), and previous MRI studies have shown a corresponding increase in T_2 and T_2-weighted signal intensity in sclerotic hippocampi (Berkovic et al., 1991, Bronen et al., 1991, Jackson et al., 1990, Jackson et al., 1993). In the current study, the combined regression analysis revealed significant HS-associated T_2 prolongation, with one of the clusters located strikingly close to, if not within, the CA1 subregion. In addition, a cluster of significant T_2 prolongation was detected in the anterior portion of the temporal lobe white matter, where there have been at least two reports of tissue abnormalities associated with HS (McMillan et al., 2004, Meiners et al., 2000).

4.4 Clinical Significance of T_2 Alterations

To the best of our knowledge, this study is the first to show spatial distributions of T_2 alterations associated with different types of neuropathology observed postmortem. These findings suggest that T_2 alterations may serve as a useful biomarker of pathology, complementing neuropsychological assessment and other testing techniques to improve the accuracy of clinical diagnosis. In addition to its associations with pathology, T_2 prolongation was shown to contribute a substantial percentage of variation in episodic, semantic, and working memory scores among participants – at least 5.5% in each domain (Table 4). These findings imply that the T_2 prolongation may reflect underlying pathologic processes not already captured by neuropathologic assessment. Conversely, the lack of significant association between T_2 shortening and cognition suggests that any related cognitive deficits were largely explained by the direct measures of neuropathology. Because of the methodology for this portion of the analysis, one concern is that worsening of neuropathology or other age-related events occurring between the final cognitive assessment and death may have affected the prominence of associations between cognition and ex vivo T_2. However, this interval was relatively short on average, and results of a secondary analysis that excluded the 22% of participants who had a lag of more than one year between cognitive assessment and death were unremarkable compared to the full analysis.

4.5 Generalization of Ex Vivo Findings

Based on previous work, we anticipated ex vivo T_2 values in fixed brain tissue to be approximately 50% of those found in vivo (Dawe et al., 2009), and this was supported by the comparison of 28 in vivo T_2 maps against 28 ex vivo T_2 maps from matched participants. Furthermore, this comparison revealed positive correlations between in vivo and ex vivo T_2 in several brain regions, indicating that findings of the current analysis may potentially be generalized to the in vivo case. As suggested by Figure 7, the precise relationship between ex vivo T_2 and in vivo T_2 is likely to vary across regions. Yet, because voxelwise analysis allows for spatial variation, regional differences in the in vivo-ex vivo T_2 relationship do not preclude the generalization of ex vivo findings to the in vivo case.

Additional investigation using in vivo and ex vivo MRI data from the same individuals is necessary to accurately describe the in vivo-ex vivo T_2 relationship throughout the brain.

4.6 Strengths and Limitations

This study employed a voxel-based approach, rather than an ROI-based approach, facilitating detection of T_2 alterations related to AD and other pathologies throughout the cerebral hemisphere. As such, spatial normalization of individual hemispheres was required. Despite ART's ranking as one of the top neuroimaging registration tools (Klein et al., 2009), differences in hemisphere anatomy, shape, size, and contrast preclude perfect spatial normalization, potentially contributing to false positives and false negatives, a limitation of the current work.

Three different scanners and pulse sequences were used to acquire T_2 data. This was necessary because of the ongoing nature of postmortem MRI data collection – the 371 hemispheres included in the full analysis were imaged over a span of approximately five years. In the voxelwise regression models, we accounted for a possible constant offset in T_2 values among the three scanners and pulse sequences, but we did not include any interaction terms to model, for example, scanner-specific disease effects. We recognized that using a single scanner and pulse sequence would be the most reliable method of eliminating scanner-to-scanner variation in T_2 values. Therefore, we repeated the entire analysis using only the 188 hemispheres that were imaged on the Philips Achieva scanner (the largest subgroup, see Table 2), and the results were overwhelmingly similar to the full 371-hemisphere analysis.

Finally, laterality was not a primary consideration of the current work, as left and right cerebral hemispheres were combined in the analyses in order to maximize degrees of freedom. Left-right asymmetry in the substrates of pathology, cognition, and T_2 alterations could have obscured otherwise significant associations among those factors. Therefore, we repeated the analysis for left and right hemispheres separately. Significant T_2 associations with pathology were similar between left and right hemispheres, though less extensive than those revealed by the full analysis, probably due to the lower power. T_2 associations with cognition (after controlling for pathology) were rendered largely non-significant in the separate left-right analyses. However, sub-significant trends did show a degree of laterality, especially in the semantic memory domain, suggesting that further investigation in this area is warranted.

Supplementary Material

Refer to Web version on PubMed Central for supplementary material.

Acknowledgments

We thank the participants of the Rush Memory and Aging Project and the Religious Orders Study. We also thank the reviewers of this manuscript for their valuable comments.

Funding

This work was supported by the National Institute on Aging [grant numbers P30 AG10161, R01 AG15819, and R01 AG17917] and by the Alzheimer's Disease Research Fund of the Illinois Department of Public Health.

References

Ardekani BA, Guckemus S, Bachman A, Hoptman MJ, Wojtaszek M, Nierenberg J. Quantitative comparison of algorithms for inter-subject registration of 3D volumetric brain MRI scans. J. Neurosci. Methods. 2005; 142:67–76. [PubMed: 15652618]

Arfanakis K, Gui M, Tamhane A, Carew J. Investigating the Medial Temporal Lobe in Alzheimer's Disease and Mild Cognitive Impairment, with Turboprop Diffusion Tensor Imaging, MRI-volumetry, and T_2-relaxometry. Brain Imaging Behav. 2007; 1:11–21.

Arvanitakis Z, Leurgans SE, Wang Z, Wilson RS, Bennett DA, Schneider JA. Cerebral amyloid angiopathy pathology and cognitive domains in older persons. Ann. Neurol. 2011; 69:320–327. [PubMed: 21387377]

Auriel E, Bornstein NM, Berenyi E, Varkonyi I, Gabor M, Majtenyi K, Szepesi R, Goldberg I, Lampe R, Csiba L. Clinical, radiological and pathological correlates of leukoaraiosis. Acta Neurol. Scand. 2011; 123:41–47. [PubMed: 20219022]

Bartzokis G, Cummings JL, Sultzer D, Henderson VW, Nuechterlein KH, Mintz J. White matter structural integrity in healthy aging adults and patients with Alzheimer disease: a magnetic resonance imaging study. Arch. Neurol. 2003; 60:393–398. [PubMed: 12633151]

Bartzokis G, Sultzer D, Cummings J, Holt LE, Hance DB, Henderson VW, Mintz J. In vivo evaluation of brain iron in Alzheimer disease using magnetic resonance imaging. Arch. Gen. Psychiatry. 2000; 57:47–53. [PubMed: 10632232]

Bartzokis G, Sultzer D, Mintz J, Holt LE, Marx P, Phelan CK, Marder SR. In vivo evaluation of brain iron in Alzheimer's disease and normal subjects using MRI. Biol. Psychiatry. 1994; 35:480–487. [PubMed: 8018799]

Bartzokis G, Tishler TA. MRI evaluation of basal ganglia ferritin iron and neurotoxicity in Alzheimer's and Huntingon's disease. Cell. Mol. Biol. (Noisy-le-grand). 2000; 46:821–833. [PubMed: 10875443]

Bennett DA, De Jager PL, Leurgans SE, Schneider JA. Neuropathologic intermediate phenotypes enhance association to Alzheimer susceptibility alleles. Neurology. 2009; 72:1495–1503. [PubMed: 19398704]

Bennett DA, Schneider JA, Arvanitakis Z, Kelly JF, Aggarwal NT, Shah RC, Wilson RS. Neuropathology of older persons without cognitive impairment from two community-based studies. Neurology. 2006; 66:1837–1844. [PubMed: 16801647]

Bennett DA, Schneider JA, Arvanitakis Z, Wilson RS. Overview and findings from the religious orders study. Curr. Alzheimer Res. 2012a; 9:628–645. [PubMed: 22471860]

Bennett DA, Schneider JA, Buchman AS, Barnes LL, Boyle PA, Wilson RS. Overview and findings from the rush Memory and Aging Project. Curr. Alzheimer Res. 2012b; 9:646–663. [PubMed: 22471867]

Berkovic SF, Andermann F, Olivier A, Ethier R, Melanson D, Robitaille Y, Kuzniecky R, Peters T, Feindel W. Hippocampal sclerosis in temporal lobe epilepsy demonstrated by magnetic resonance imaging. Ann. Neurol. 1991; 29:175–182. [PubMed: 2012385]

Besson JA, Best PV, Skinner ER. Post-mortem proton magnetic resonance spectrometric measures of brain regions in patients with a pathological diagnosis of Alzheimer's disease and multi-infarct dementia. Br. J. Psychiatry. 1992; 160:187–190. [PubMed: 1540758]

Bozzali M, Falini A, Franceschi M, Cercignani M, Zuffi M, Scotti G, Comi G, Filippi M. White matter damage in Alzheimer's disease assessed in vivo using diffusion tensor magnetic resonance imaging. J. Neurol. Neurosurg. Psychiatry. 2002; 72:742–746. [PubMed: 12023417]

Bozzali M, Giulietti G, Basile B, Serra L, Spano B, Perri R, Giubilei F, Marra C, Caltagirone C, Cercignani M. Damage to the cingulum contributes to alzheimer's disease pathophysiology by deafferentation mechanism. Hum. Brain Mapp. 2012; 33:1295–1308. [PubMed: 21520352]

Bronen RA, Cheung G, Charles JT, Kim JH, Spencer DD, Spencer SS, Sze G, McCarthy G. Imaging findings in hippocampal sclerosis: correlation with pathology. AJNR Am. J. Neuroradiol. 1991; 12:933–940. [PubMed: 1950925]

Brun A, Englund E. A white matter disorder in dementia of the Alzheimer type: a pathoanatomical study. Ann. Neurol. 1986; 19:253–262. [PubMed: 3963770]

Choo IH, Lee DY, Oh JS, Lee JS, Lee DS, Song IC, Youn JC, Kim SG, Kim KW, Jhoo JH, Woo JI. Posterior cingulate cortex atrophy and regional cingulum disruption in mild cognitive impairment and Alzheimer's disease. Neurobiol. Aging. 2010; 31:772–779. [PubMed: 18687503]

Cox RW. AFNI: software for analysis and visualization of functional magnetic resonance neuroimages. Comput. Biomed. Res. 1996; 29:162–173. [PubMed: 8812068]

Dawe RJ, Bennett DA, Schneider JA, Arfanakis K. Neuropathologic correlates of hippocampal atrophy in the elderly: a clinical, pathologic, postmortem MRI study. PLoS One. 2011; 6:e26286. [PubMed: 22043314]

Dawe RJ, Bennett DA, Schneider JA, Vasireddi SK, Arfanakis K. Postmortem MRI of human brain hemispheres: T2 relaxation times during formaldehyde fixation. Magn. Reson. Med. 2009; 61:810–818. [PubMed: 19189294]

Dickson DW, Davies P, Bevona C, Van Hoeven KH, Factor SM, Grober E, Aronson MK, Crystal HA. Hippocampal sclerosis: a common pathological feature of dementia in very old (> or = 80 years of age) humans. Acta Neuropathol. 1994; 88:212–221. [PubMed: 7810292]

Englund E. Neuropathology of white matter changes in Alzheimer's disease and vascular dementia. Dement. Geriatr. Cogn. Disord. 1998; 9(Suppl 1):6–12. [PubMed: 9716238]

Englund E, Brun A, Alling C. White matter changes in dementia of Alzheimer's type. Biochemical and neuropathological correlates. Brain. 1988; 111(Pt 6):1425–1439. [PubMed: 3208064]

Englund E, Brun A, Persson B. Correlations between histopathologic white matter changes and proton MR relaxation times in dementia. Alzheimer Dis. Assoc. Disord. 1987; 1:156–170. [PubMed: 3453747]

Fazekas F, Kleinert R, Offenbacher H, Schmidt R, Kleinert G, Payer F, Radner H, Lechner H. Pathologic correlates of incidental MRI white matter signal hyperintensities. Neurology. 1993; 43:1683–1689. [PubMed: 8414012]

Fellgiebel A, Muller MJ, Wille P, Dellani PR, Scheurich A, Schmidt LG, Stoeter P. Color-coded diffusion-tensor-imaging of posterior cingulate fiber tracts in mild cognitive impairment. Neurobiol. Aging. 2005; 26:1193–1198. [PubMed: 15917103]

Fernando MS, O'Brien JT, Perry RH, English P, Forster G, McMeekin W, Slade JY, Golkhar A, Matthews FE, Barber R, Kalaria RN, Ince PG. Neuropathology Group of MRC CFAS. Comparison of the pathology of cerebral white matter with post-mortem magnetic resonance imaging (MRI) in the elderly brain. Neuropathol. Appl. Neurobiol. 2004; 30:385–395. [PubMed: 15305984]

Fernando MS, Simpson JE, Matthews F, Brayne C, Lewis CE, Barber R, Kalaria RN, Forster G, Esteves F, Wharton SB, Shaw PJ, O'Brien JT, Ince PG. MRC Cognitive Function and Ageing Neuropathology Study Group. White matter lesions in an unselected cohort of the elderly: molecular pathology suggests origin from chronic hypoperfusion injury. Stroke. 2006; 37:1391–1398. [PubMed: 16627790]

Haacke EM, Cheng NY, House MJ, Liu Q, Neelavalli J, Ogg RJ, Khan A, Ayaz M, Kirsch W, Obenaus A. Imaging iron stores in the brain using magnetic resonance imaging. Magn. Reson. Imaging. 2005; 23:1–25. [PubMed: 15733784]

Hanyu H, Sakurai H, Iwamoto T, Takasaki M, Shindo H, Abe K. Diffusion-weighted MR imaging of the hippocampus and temporal white matter in Alzheimer's disease. J. Neurol. Sci. 1998; 156:195–200. [PubMed: 9588857]

Hasan KM, Walimuni IS, Kramer LA, Frye RE. Human brain atlas-based volumetry and relaxometry: application to healthy development and natural aging. Magn. Reson. Med. 2010; 64:1382–1389. [PubMed: 20740662]

House MJ, St Pierre TG, Foster JK, Martins RN, Clarnette R. Quantitative MR imaging R2 relaxometry in elderly participants reporting memory loss. AJNR Am. J. Neuroradiol. 2006; 27:430–439. [PubMed: 16484425]

House MJ, St Pierre TG, McLean C. 1.4T study of proton magnetic relaxation rates, iron concentrations, and plaque burden in Alzheimer's disease and control postmortem brain tissue. Magn. Reson. Med. 2008; 60:41–52. [PubMed: 18523986]

Huang J, Friedland RP, Auchus AP. Diffusion tensor imaging of normal-appearing white matter in mild cognitive impairment and early Alzheimer disease: preliminary evidence of axonal degeneration in the temporal lobe. AJNR Am. J. Neuroradiol. 2007; 28:1943–1948. [PubMed: 17905894]

Inzitari D. Leukoaraiosis: an independent risk factor for stroke? Stroke. 2003; 34:2067–2071. [PubMed: 12829859]

Jackson GD, Berkovic SF, Duncan JS, Connelly A. Optimizing the diagnosis of hippocampal sclerosis using MR imaging. AJNR Am. J. Neuroradiol. 1993; 14:753–762. [PubMed: 8517369]

Jackson GD, Berkovic SF, Tress BM, Kalnins RM, Fabinyi GC, Bladin PF. Hippocampal sclerosis can be reliably detected by magnetic resonance imaging. Neurology. 1990; 40:1869–1875. [PubMed: 2247236]

Joshi S, Davis B, Jomier M, Gerig G. Unbiased diffeomorphic atlas construction for computational anatomy. Neuroimage. 2004; 23(Suppl 1):S151–S160. [PubMed: 15501084]

Kirsch SJ, Jacobs RW, Butcher LL, Beatty J. Prolongation of magnetic resonance T2 time in hippocampus of human patients marks the presence and severity of Alzheimer's disease. Neurosci. Lett. 1992; 134:187–190. [PubMed: 1589144]

Klein A, Andersson J, Ardekani BA, Ashburner J, Avants B, Chiang MC, Christensen GE, Collins DL, Gee J, Hellier P, Song JH, Jenkinson M, Lepage C, Rueckert D, Thompson P, Vercauteren T, Woods RP, Mann JJ, Parsey RV. Evaluation of 14 nonlinear deformation algorithms applied to human brain MRI registration. Neuroimage. 2009; 46:786–802. [PubMed: 19195496]

Kumar R, Delshad S, Woo MA, Macey PM, Harper RM. Age-related regional brain T2-relaxation changes in healthy adults. J. Magn. Reson. Imaging. 2012; 35:300–308. [PubMed: 21987489]

Laakso MP, Partanen K, Soininen H, Lehtovirta M, Hallikainen M, Hanninen T, Helkala EL, Vainio P, Riekkinen PJS. MR T2 relaxometry in Alzheimer's disease and age-associated memory impairment. Neurobiol. Aging. 1996; 17:535–540. [PubMed: 8832627]

Loeffler DA, Connor JR, Juneau PL, Snyder BS, Kanaley L, DeMaggio AJ, Nguyen H, Brickman CM, LeWitt PA. Transferrin and iron in normal, Alzheimer's disease, and Parkinson's disease brain regions. J. Neurochem. 1995; 65:710–724. [PubMed: 7616227]

Lovell MA, Robertson JD, Teesdale WJ, Campbell JL, Markesbery WR. Copper, iron and zinc in Alzheimer's disease senile plaques. J. Neurol. Sci. 1998; 158:47–52. [PubMed: 9667777]

McKeith IG. Consensus guidelines for the clinical and pathologic diagnosis of dementia with Lewy bodies (DLB): report of the Consortium on DLB International Workshop. J. Alzheimers Dis. 2006; 9:417–423. [PubMed: 16914880]

McMillan AB, Hermann BP, Johnson SC, Hansen RR, Seidenberg M, Meyerand ME. Voxel-based morphometry of unilateral temporal lobe epilepsy reveals abnormalities in cerebral white matter. Neuroimage. 2004; 23:167–174. [PubMed: 15325363]

Meiners LC, van der Grond J, van Rijen PC, Springorum R, de Kort GA, Jansen GH. Proton magnetic resonance spectroscopy of temporal lobe white matter in patients with histologically proven hippocampal sclerosis. J. Magn. Reson. Imaging. 2000; 11:25–31. [PubMed: 10676617]

Mielke MM, Kozauer NA, Chan KC, George M, Toroney J, Zerrate M, Bandeen-Roche K, Wang MC, Vanzijl P, Pekar JJ, Mori S, Lyketsos CG, Albert M. Regionally-specific diffusion tensor imaging in mild cognitive impairment and Alzheimer's disease. Neuroimage. 2009; 46:47–55. [PubMed: 19457371]

Roher AE, Weiss N, Kokjohn TA, Kuo YM, Kalback W, Anthony J, Watson D, Luehrs DC, Sue L, Walker D, Emmerling M, Goux W, Beach T. Increased A beta peptides and reduced cholesterol and myelin proteins characterize white matter degeneration in Alzheimer's disease. Biochemistry. 2002; 41:11080–11090. [PubMed: 12220172]

Rombouts SA, Scheltens P, Kuijer JP, Barkhof F. Whole brain analysis of T2* weighted baseline FMRI signal in dementia. Hum. Brain Mapp. 2007; 28:1313–1317. [PubMed: 17290368]

Schneider JA, Arvanitakis Z, Leurgans SE, Bennett DA. The neuropathology of probable Alzheimer disease and mild cognitive impairment. Ann. Neurol. 2009; 66:200–208. [PubMed: 19743450]

Schneider JA, Boyle PA, Arvanitakis Z, Bienias JL, Bennett DA. Subcortical infarcts, Alzheimer's disease pathology, and memory function in older persons. Ann. Neurol. 2007; 62:59–66. [PubMed: 17503514]

Sjobeck M, Englund E. Glial levels determine severity of white matter disease in Alzheimer's disease: a neuropathological study of glial changes. Neuropathol. Appl. Neurobiol. 2003; 29:159–169. [PubMed: 12662323]

Smith MA, Harris PL, Sayre LM, Perry G. Iron accumulation in Alzheimer disease is a source of redox-generated free radicals. Proc. Natl. Acad. Sci. U.S.A. 1997; 94:9866–9868. [PubMed: 9275217]

Soderberg M, Edlund C, Alafuzoff I, Kristensson K, Dallner G. Lipid composition in different regions of the brain in Alzheimer's disease/senile dementia of Alzheimer's type. J. Neurochem. 1992; 59:1646–1653. [PubMed: 1402910]

Takahashi S, Yonezawa H, Takahashi J, Kudo M, Inoue T, Tohgi H. Selective reduction of diffusion anisotropy in white matter of Alzheimer disease brains measured by 3.0 Tesla magnetic resonance imaging. Neurosci. Lett. 2002; 332:45–48. [PubMed: 12377381]

Taoka T, Iwasaki S, Sakamoto M, Nakagawa H, Fukusumi A, Myochin K, Hirohashi S, Hoshida T, Kichikawa K. Diffusion anisotropy and diffusivity of white matter tracts within the temporal stem in Alzheimer disease: evaluation of the "tract of interest" by diffusion tensor tractography. AJNR Am. J. Neuroradiol. 2006; 27:1040–1045. [PubMed: 16687540]

The National Institute on Aging, and Reagan Institute Working Group on Diagnostic Criteria for the Neuropathological Assessment of Alzheimer's Disease. Consensus recommendations for the postmortem diagnosis of Alzheimer's disease. Neurobiol. Aging. 1997; 18:S1–S2. [PubMed: 9330978]

Wang H, Yuan H, Shu L, Xie J, Zhang D. Prolongation of T(2) relaxation times of hippocampus and amygdala in Alzheimer's disease. Neurosci. Lett. 2004; 363:150–153. [PubMed: 15172104]

Wang Y, West JD, Flashman LA, Wishart HA, Santulli RB, Rabin LA, Pare N, Arfanakis K, Saykin AJ. Selective changes in white matter integrity in MCI and older adults with cognitive complaints. Biochim. Biophys. Acta. 2012; 1822:423–430. [PubMed: 21867750]

Watt F. Nuclear microscope analysis in Alzheimer's and Parkinson's disease: A review. Cell. Mol. Biol. (Noisy-le-grand). 1996; 42:17–26. [PubMed: 8833663]

West MJ, Coleman PD, Flood DG, Troncoso JC. Differences in the pattern of hippocampal neuronal loss in normal ageing and Alzheimer's disease. Lancet. 1994; 344:769–772. [PubMed: 7916070]

Wilson RS, Schneider JA, Boyle PA, Arnold SE, Tang Y, Bennett DA. Chronic distress and incidence of mild cognitive impairment. Neurology. 2007; 68:2085–2092. [PubMed: 17562829]

Xie S, Xiao JX, Gong GL, Zang YF, Wang YH, Wu HK, Jiang XX. Voxel-based detection of white matter abnormalities in mild Alzheimer disease. Neurology. 2006; 66:1845–1849. [PubMed: 16801648]

Zhang Y, Schuff N, Jahng GH, Bayne W, Mori S, Schad L, Mueller S, Du AT, Kramer JH, Yaffe K, Chui H, Jagust WJ, Miller BL, Weiner MW. Diffusion tensor imaging of cingulum fibers in mild cognitive impairment and Alzheimer disease. Neurology. 2007; 68:13–19. [PubMed: 17200485]

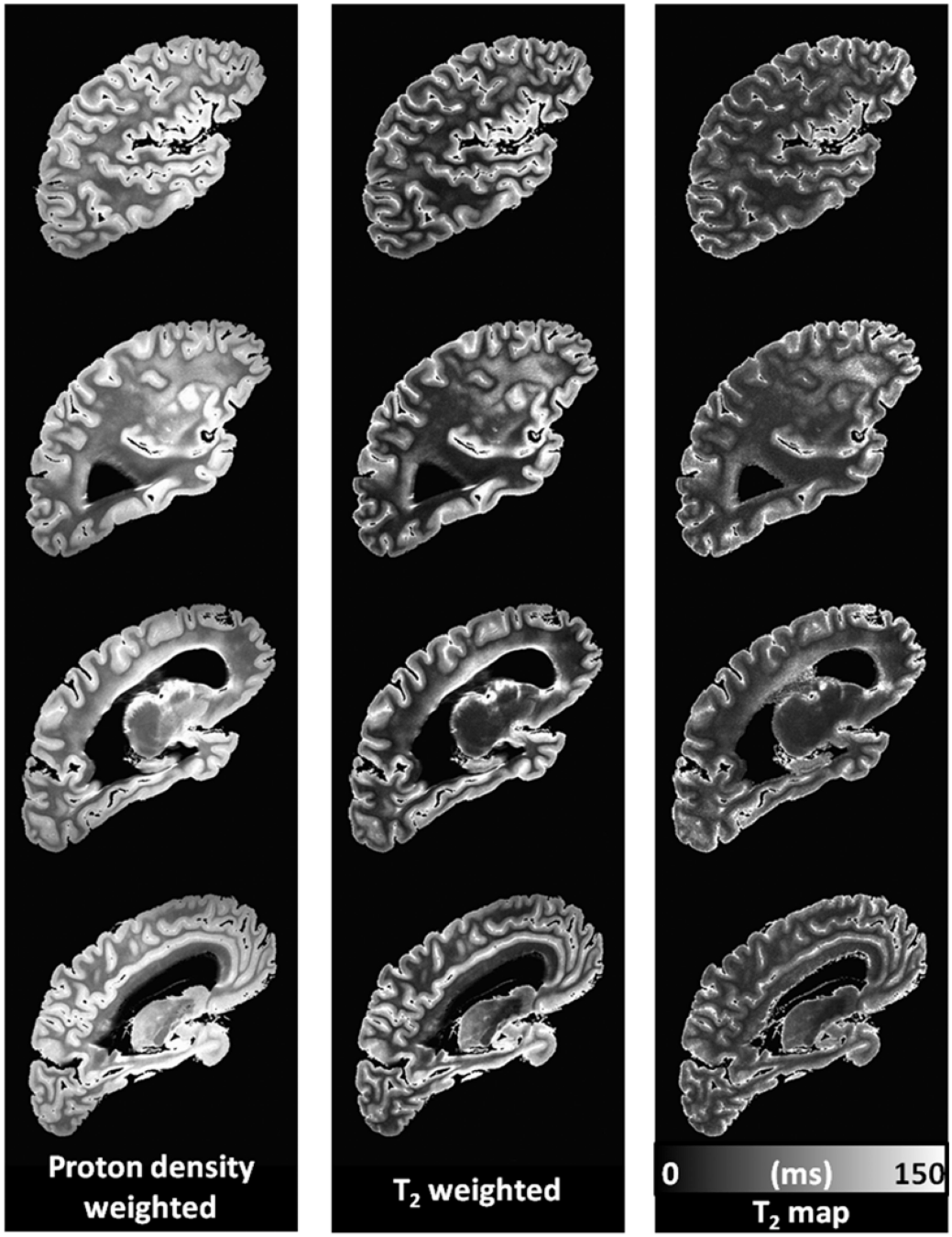

Figure 1.

Slices from a typical masked proton density-weighted image volume (TE = 13 ms), a T_2-weighted image volume (TE = 52 ms), and estimated T_2 map from an individual postmortem cerebral hemisphere, shown in the same orientation and resolution as the natively acquired sagittal slices.

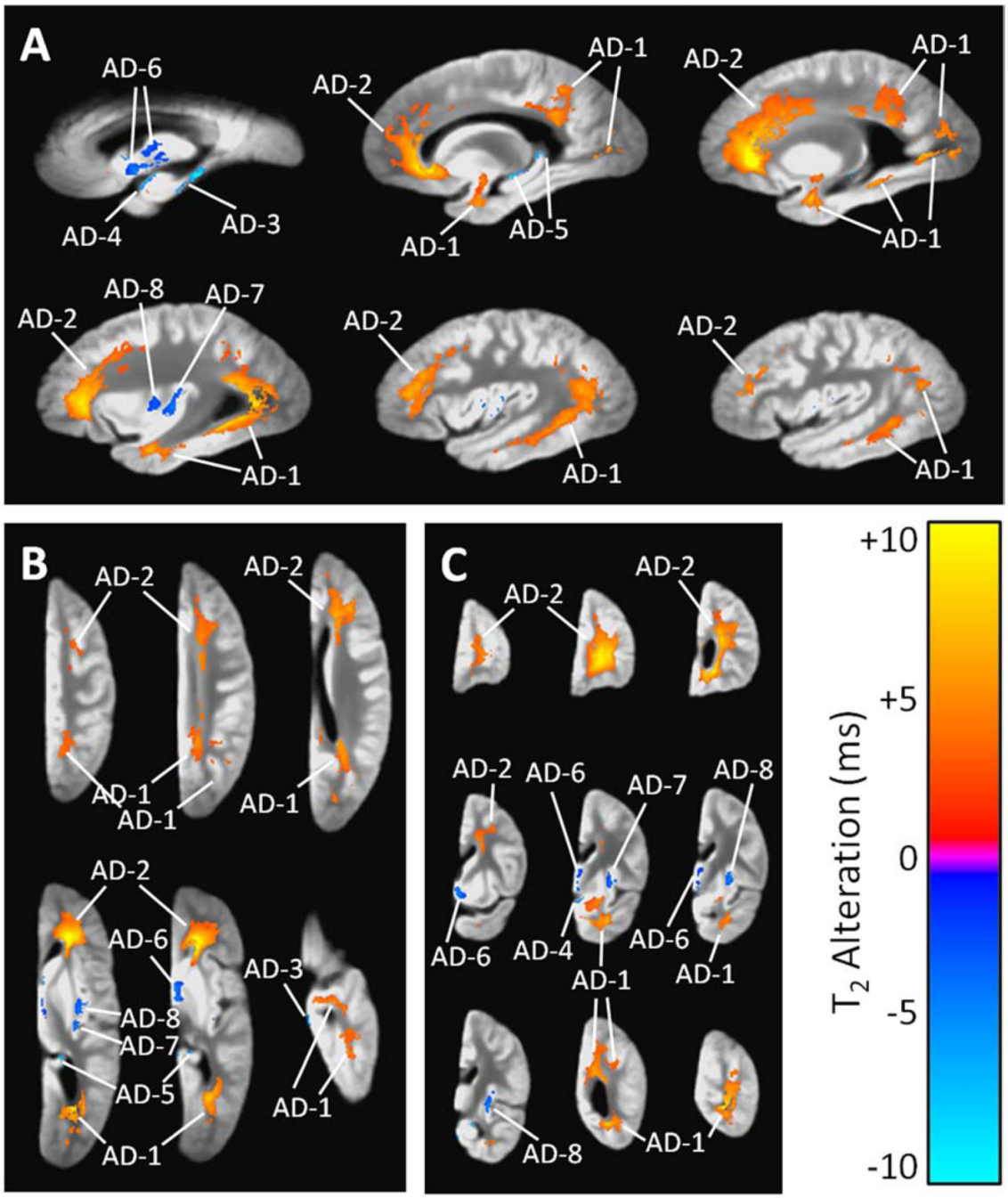

Figure 2.

(A) Sagittal, (B) axial, and (C) coronal views showing regions of significant T_2 prolongation (orange) and T_2 shortening (blue) associated with a high summary score of AD pathology, according to a combined linear regression analysis that simultaneously considered AD pathology, acute and chronic gross infarcts, and hippocampal sclerosis (and covariates). The grayscale underlay is the study-specific template (proton density-weighted). Alphanumeric labels are those cluster identifiers introduced in Table 3.

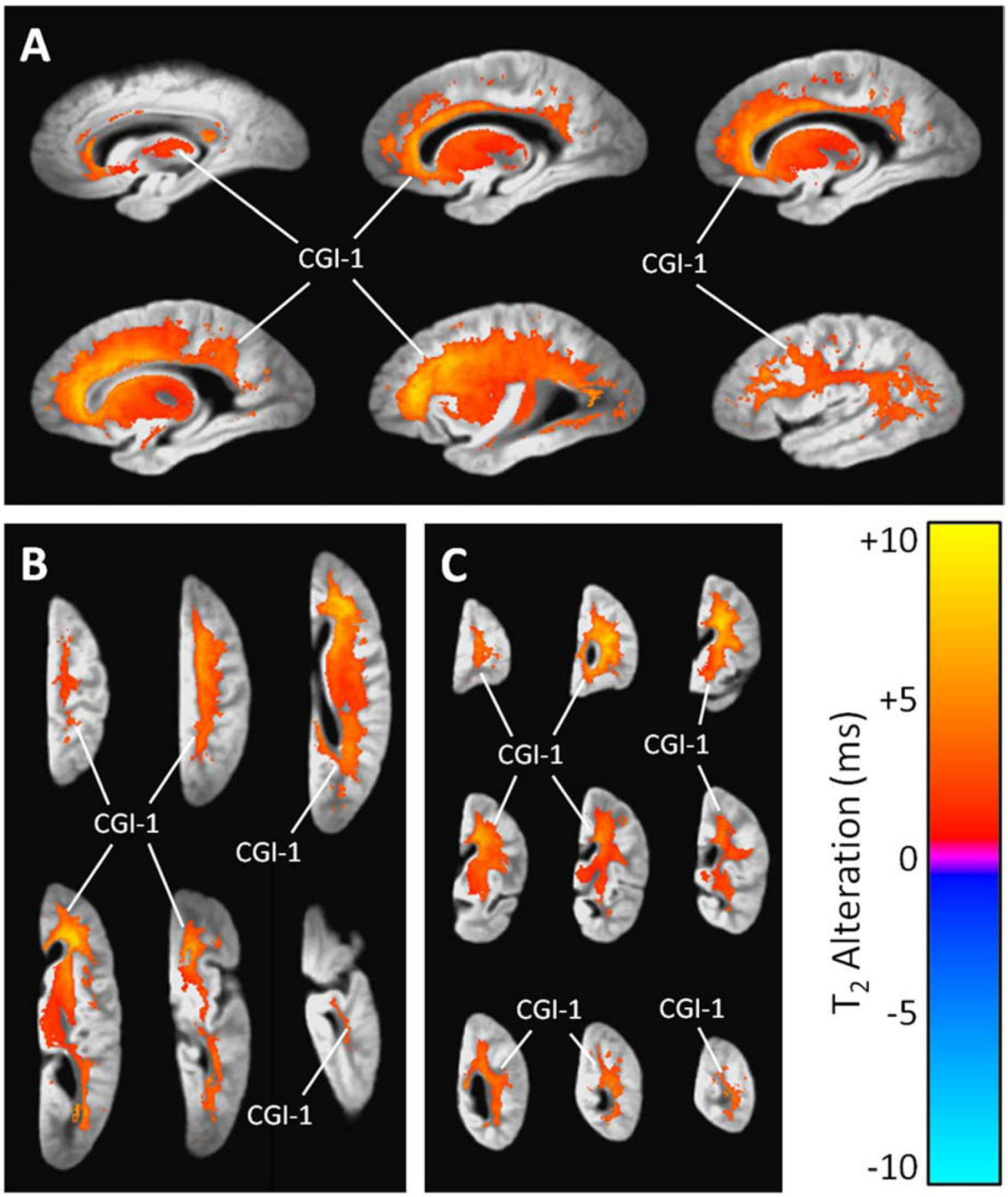

Figure 3.

(A) Sagittal, (B) axial, and (C) coronal views showing regions of significant T_2 prolongation and T_2 shortening associated with the number of chronic gross infarcts per cerebral hemisphere, according to a combined linear regression analysis that simultaneously considered AD pathology, acute and chronic gross infarcts, and hippocampal sclerosis (and covariates). The grayscale underlay is the study-specific template (proton density-weighted). Alphanumeric labels are those cluster identifiers introduced in Table 3.

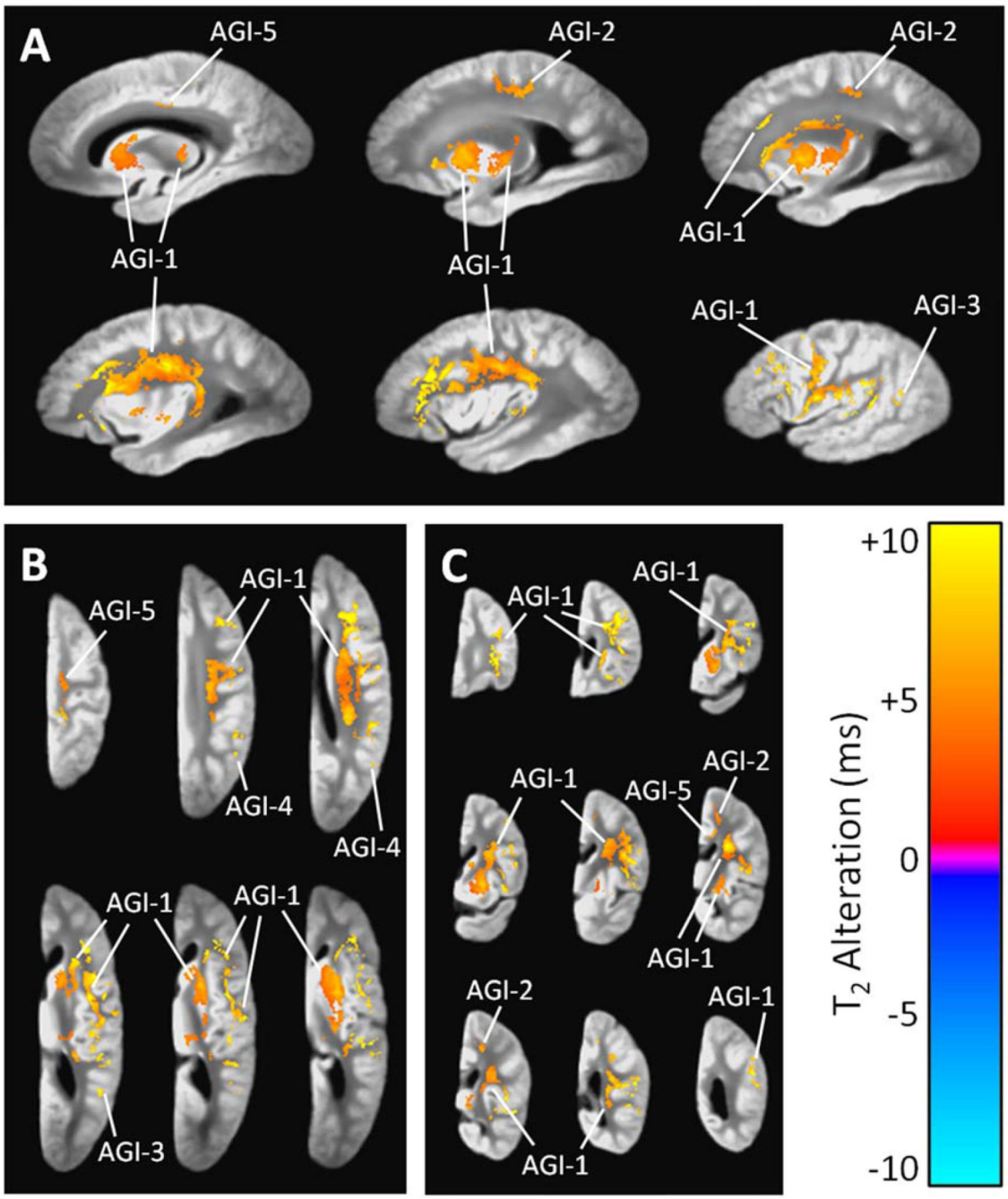

Figure 4.

(A) Sagittal, (B) axial, and (C) coronal views showing regions of significant T_2 prolongation and T_2 shortening associated with the number of acute gross infarcts per cerebral hemisphere, according to a combined linear regression analysis that simultaneously considered AD pathology, acute and chronic gross infarcts, and hippocampal sclerosis (and covariates). The grayscale underlay is the study-specific template (proton density-weighted). Alphanumeric labels are those cluster identifiers introduced in Table 3.

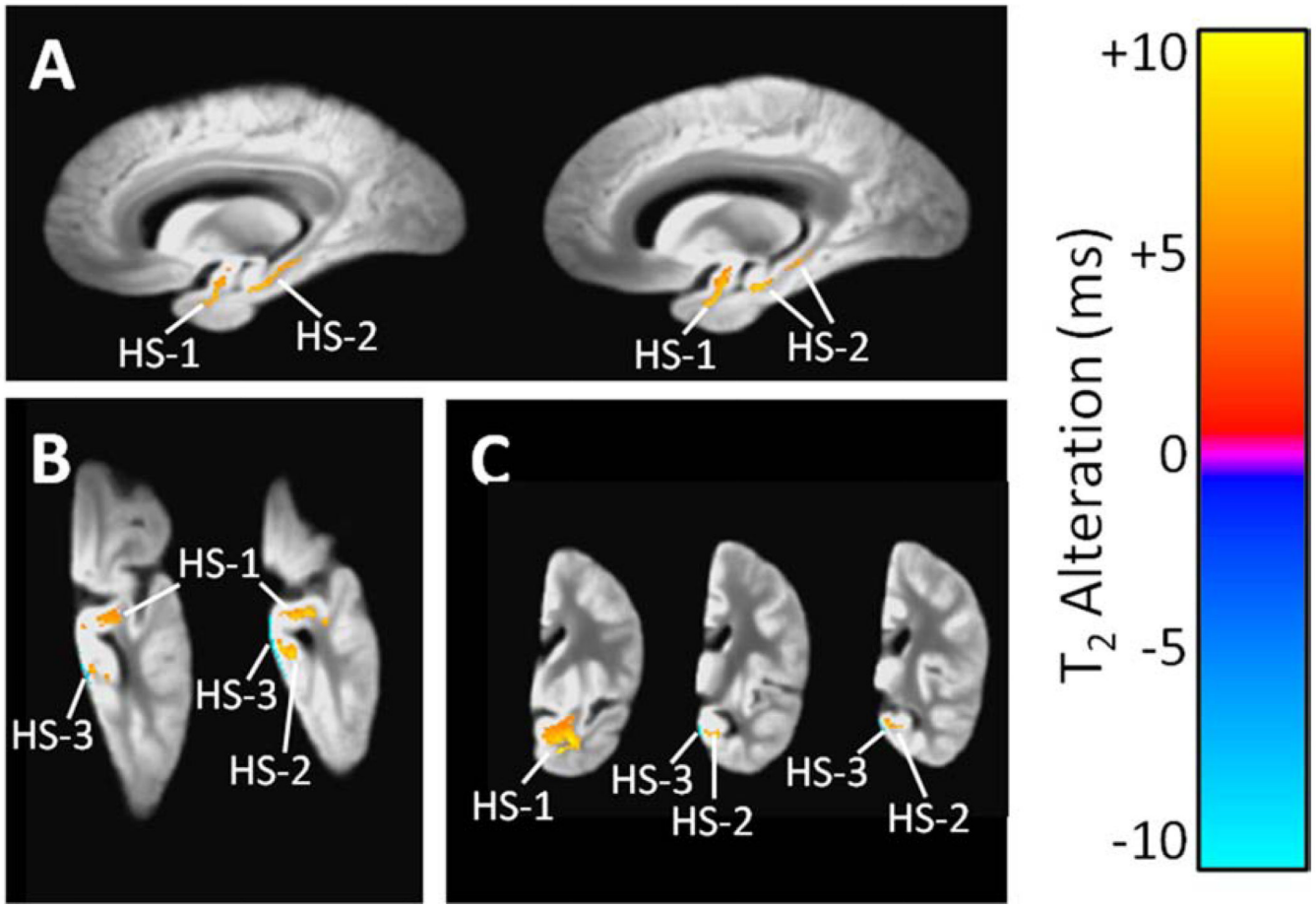

Figure 5.

(A) Sagittal, (B) axial, and (C) coronal views region of significant T_2 prolongation associated with hippocampal sclerosis, according to a combined linear regression analysis that simultaneously considered AD pathology, acute and chronic gross infarcts, and hippocampal sclerosis (and covariates). The grayscale underlay is the study-specific template (proton density-weighted). Alphanumeric labels are those cluster identifiers introduced in Table 3.

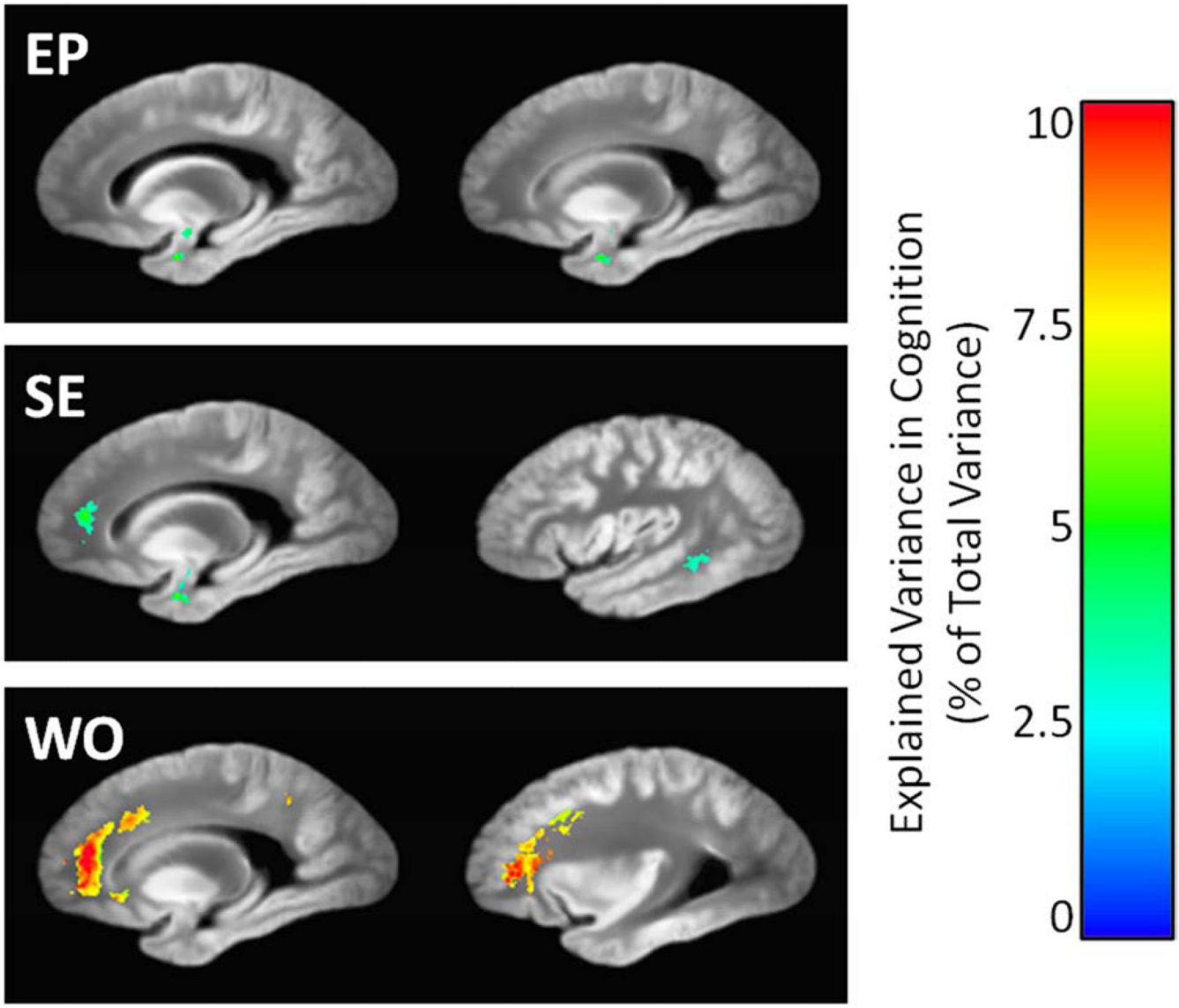

Figure 6.

Sagittal views of the regions in which episodic memory (EP), semantic memory (SE), and working memory (WO) deficits were significantly associated with T_2 prolongation, according to linear regression models that also considered neuropathology measures and demographic covariates. Colors indicate the amount of additional variance in working memory explained by T_2, beyond that accounted for by neuropathology and demographics. The grayscale underlay is the study-specific template (proton density-weighted).

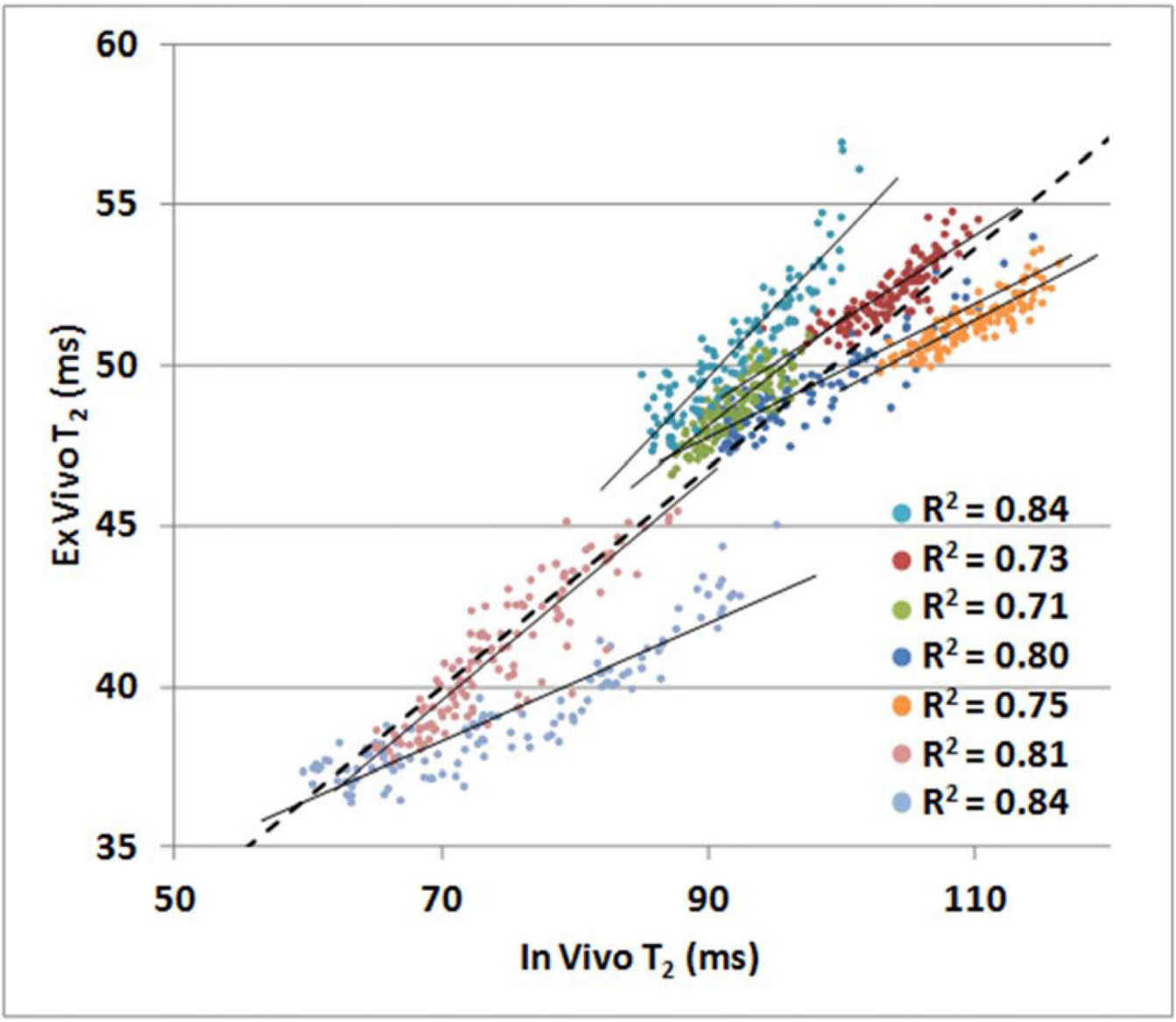

Figure 7.

Ex vivo T_2 values versus in vivo T_2 values for corresponding voxels within seven regions of interest located in white matter and subcortical gray matter (one color per region). The mean ex vivo T_2 value for a given voxel was calculated across 28 ex vivo hemispheres registered to a template. The mean in vivo T_2 value for each voxel was calculated across 28 in vivo hemispheres registered to the same template. Slopes for all regression lines were significantly positive (R^2 values displayed, $p < 10^{-15}$ for all).

Table 1

Fast spin-echo sequences from each of three MRI scanners employed in the current study.

	GE Signa 3T	Siemens Trio 3T	Philips Achieva 3T
Subjects scanned	95	88	188
FOV (mm)	160 × 160	160 × 160	160 × 160
Acquisition matrix	256 × 256	256 × 256	260 × 258
Slice thickness (mm)	1.5	1.5	1.5
Native voxel dimensions (mm)	0.625 × 0.625 × 1.5	0.625 × 0.625 × 1.5	0.615 × 0.620 × 1.5
Native voxel volume (mm^3)	0.59	0.59	0.57
Echo Times (ms)	13, 52	12, 35, 58	16.5, 33, 49.5, 66, 82.5
TR (ms)	3600	3750	4055
ETL	6	2	5
NEX	6	4	2
Scan time (min)	31	32	35

Table 2

Selected demographic and neuropathologic characteristics of 371 cerebral hemispheres.

Total number of subjects, n	371
Specimen source	
--Memory and Aging Project (MAP), n (%)	229 (62%)
--Religious Orders Study (ROS), n (%)	142 (38%)
MRI scanner, n (%)	
--GE	95 (26%)
--Siemens	88 (24%)
--Philips	188 (51%)
Age at death, y (SD)	89.6 (6.2)
Sex, n (%)	
--Male	111 (30%)
--Female	260 (70%)
Education, y (SD)	15.9 (3.6)
Right hemisphere, n (%)	175 (47%)
Postmortem interval to imaging, days (SD)	46.9 (25.4)
NIA Reagan (AD pathology), n (%)	
--None or low	126 (34%)
--Intermediate	168 (45%)
--High	77 (21%)
Lewy bodies, n (%)	
--Limbic	33 (9%)
--Neocortical	42 (11%)
--Total, any location	75 (20%)
Gross infarcts, n (%)	
--Chronic, only one	61 (16%)
--Chronic, more than one	67 (18%)
--Subacute, only one	42 (11%)
--Subacute, more than one	11 (3%)
--Acute, only one	15 (4%)
--Acute, more than one	6 (2%)
Microscopic infarcts, n (%)	
--Chronic, only one	70 (19%)
--Chronic, more than one	38 (10%)
--Subacute, only one	21 (6%)
--Subacute, more than one	4 (1%)
--Acute, only one	14 (4%)
--Acute, more than one	3 (1%)
Hippocampal sclerosis, n (%)	80 (22%)

Table 3

Clusters of 100 mm^3 or more with statistically significant T_2 alterations associated with Alzheimer's disease, gross infarcts, and hippocampal sclerosis, with all three types of neuropathology considered simultaneously.

Cluster Identifier	Principal Location	Volume (mm^3)	Mean T_2 Alteration (ms)	Minimum P-Value (unadjusted)
AD-1 [a]	Temporal, occipital, and parietal WM[b]	11,320	+4.4	2.0×10^{-4}
AD-2	Frontal WM	13,648	+3.1	1.5×10^{-3}
AD-3	Edge of temporal lobe	114	−5.8	5.0×10^{-4}
AD-4	Edge of temporal lobe	161	−5.6	2.1×10^{-3}
AD-5	Edge of hippocampus	133	−5.4	1.3×10^{-3}
AD-6	Caudate, globus pallidus, medial thalamus	594	−2.5	1.5×10^{-3}
AD-7	Insula	263	−2.8	2.9×10^{-3}
AD-8	Insula	311	−3.1	1.5×10^{-3}
CGI-1 [c]	Widespread	76,716	+2.7	4.3×10^{-3}
AGI-1 [d]	Frontal and parietal WM, putamen	19,581	+6.9	2.3×10^{-3}
AGI-2	Frontal and parietal WM	774	+5.6	2.5×10^{-3}
AGI-3	Occipital WM and GM[b]	141	+7.3	1.8×10^{-3}
AGI-4	Occipital and parietal WM and GM	136	+8.1	7.5×10^{-4}
AGI-5	Cingulum	110	+4.8	7.6×10^{-4}
HS-1 [e]	Temporal stem WM	912	+6.7	1.2×10^{-4}
HS-2	Hippocampus and parahippocampal WM	308	+6.2	1.3×10^{-4}
HS-3	Edge of temporal lobe	123	−9.1	6.0×10^{-6}

[a] AD clusters relate to the association of T_2 with the global Alzheimer's pathology score.

[b] WM = white matter, GM = gray matter.

[c] CGI cluster relates to the association of T_2 with the number of chronic gross infarcts.

[d] AGI clusters relate to the association of T_2 with the number of acute gross infarcts.

[e] HS clusters relate to the association of T_2 with the presence of hippocampal sclerosis.

Table 4

Variance in cognition explained by linear models.

Factors included in model	Cognitive domain				
	Episodic Memory	**Semantic Memory**	**Working Memory**	**Perceptual Speed**	**Visuospatial Ability**
Demographics only	4.7%	2.2%	2.7%	5.5%	10.6%
Demographics + AD	23.6	14.4	14.3	12.4	16.6
Demographics + gross infarcts	6.8	5.0	5.1	7.6	10.7
Demographics + micro infarcts	5.0	2.8	3.1	7.1	10.7
Demographics + HS	12.5	10.4	4.7	10.1	12.4
Demographics + Lewy bodies	5.7	2.9	3.4	6.1	11.5
Demographics + all pathology	31.8	24.0	18.2	19.6	18.2
Demographics + all pathology + ROI T_2 [f]	37.3	32.8	25.9	NA [g]	NA [g]
Additional variance in cognition explained by ROI T_2	5.5	8.8	7.7	NA [g]	NA [g]

All values are percentages. Each cognitive domain was assessed separately.

[f] ROI T_2 means the average value of T_2 calculated over all voxels within a cluster detected as having significant association of cognition with T_2 for a given domain. T_2 for each ROI was included as a separate factor in the model.

[g] Not applicable; there were no clusters detected as having significant associations of cognition with T_2 for these domains.